www.sciencemag.org/cgi/content/full/science.1259729/DC1

Supplementary Materials for

Chirality density wave of the "hidden order" phase in URu_2Si_2

H.-H. Kung,* R. E. Baumbach, E. D. Bauer, V. K. Thorsmølle, W.-L. Zhang, K. Haule,*
J. A. Mydosh, G. Blumberg*

*Corresponding author. E-mail: girsh@physics.rutgers.edu (G.B.); haule@physics.rutgers.edu (K.H.); skung@physics.rutgers.edu (H.-H.K.)

Published 12 February 2015 on *Science* Express
DOI: 10.1126/science.1259729

This PDF file includes:

Materials and Methods
Supplementary Text
Figs. S1 to S4
Table S1
References

Contents

S1 Material and methods **3**
- S1.1 Sample preparation . . . 3
- S1.2 Experimental methods . . . 3
- S1.3 Statistical methods . . . 4
- S1.4 Phonon width and leakage at low temperature . . . 5

S2 The dominant crystal field states of U-5*f* electrons **6**

S3 The hexadecapole order parameter **7**

S4 The low energy two-states minimal model **10**
- S4.1 Raman susceptibility in A_{2g} channel and static magnetic susceptibility along *c*-axis . . . 10
- S4.2 Effect of the magnetic field along *c*-axis in the HO phase . . . 11
- S4.3 The Raman intensity of the A_{2g} in-gap mode . . . 12
- S4.4 The "leakage" intensity of the in-gap mode into the A_{1g} channel . . . 12
- S4.5 Beyond the minimal model . . . 13
- S4.6 Leakage intensity due to broken C_4 symmetry . . . 15

S5 Magnetic torque in the ordered state with field in *xy*-plane **15**

S1 Material and methods

S1.1 Sample preparation

The Raman scattering experiments were performed from the *ab*-plane of stress free URu_2Si_2 single crystals grown by the Czochralski method and post-processed by electro-refinement (*15, 33, 34*). The *ab*-plane residual resistivity ratio for crystals from the same batch as used for this Raman scattering study are between 300-700 (*35*). The cleaved samples were examined under Nomarski microscope to find a stress free area, and the crystallographic axes were determined by Laue diffraction.

S1.2 Experimental methods

The URu_2Si_2 single crystal was cleaved and kept in vacuum before being mounted into a continuous He gas flow optical cryostat. All Raman scattering measurements were performed in a quasi-backscattering geometry along the sample *c*-axis with 752.5 nm (about 1.65 eV) excitation from a Kr^+ laser. The incident laser beam was less than 7 mW, and all reported temperatures are corrected for laser heating.

Scattered light was analyzed by a custom-designed aberration-corrected, triple-grating spectrometer equipped with master holographic gratings, imaging system, and liquid nitrogen cooled CCD detector, tailored for low frequency polarization resolved electronic Raman spectroscopy studies at low temperatures.

The spectra was corrected for the spectral response of the spectrometer and CCD to obtain the Raman intensity in the scattering geometry $\mathbf{e}_s\mathbf{e}_i$ (*36*):

$$\mathrm{I}_{\mathbf{e}_s\mathbf{e}_i}(\omega,T) = (n(\omega,T)+1)\chi''_{\mathbf{e}_s\mathbf{e}_i}(\omega,T) + L(T) \tag{S1}$$

Raman response function $\chi''(\omega,T)$ was calculated from the measured Raman intensity using Eq. S1, where $n(\omega,T)$ is the Bose-Einstein distribution function, and $L(T)$ is a small constant background resulting from luminescence of the sample and residual background of the system determined from independent reference measurements.

The scattering geometries are noted by the directional vectors of incident and scattered light polarizations: $\mathbf{e}_s\mathbf{e}_i$ =XX, XY, X′X′, X′Y′, RR and RL, where X=[100], Y=[010] are aligned along crystallographic axes, X′=[110], Y′=[1$\bar{1}$0] are aligned 45° to the *a*-axes, R=(X+iY)/$\sqrt{2}$ and L=(X-iY)/$\sqrt{2}$ are right and left circularly polarized light, respectively. For example, in the XX scattering geometry, both the incident light and scattered light polarizations are aligned parallel to the crystallographic *a*-axis. For the X′Y′ scattering geometry, the incident light polarization is orthogonal to the polarization of the scattered light, while the sample crystallographic *a*-axis is rotated 45° with respect to the incident and scattered light polarization. The residual background is different in parallel and cross scattering geometries. The ion laser plasma emission lines at 753.2 nm, 753.4 nm and 753.7 nm were fitted with a Lorentzian and then subtracted out from data.

S1.3 Statistical methods

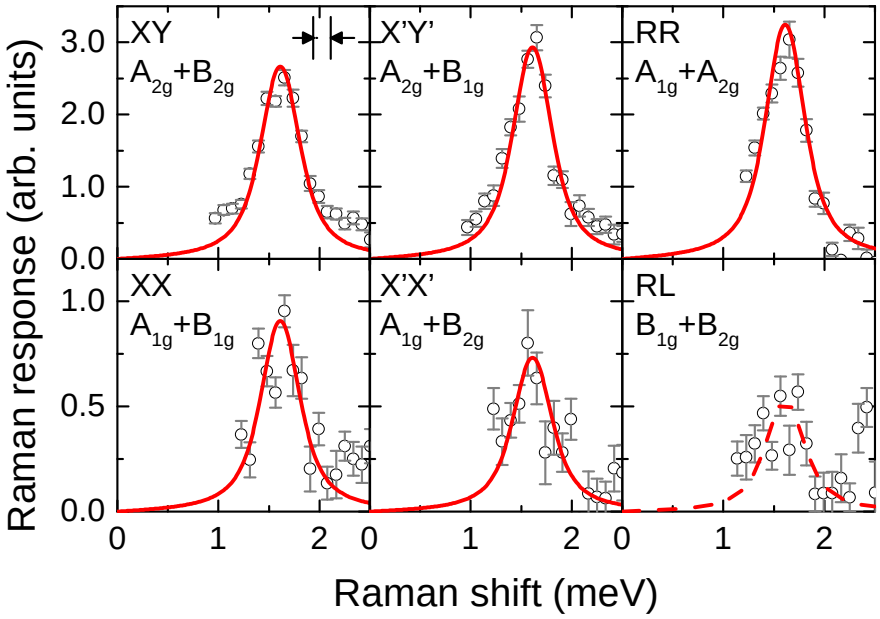

Figure S1: The Raman response in six scattering geometries at 7 K. The error bars show one standard deviation associated with each data point. The irreducible representations of the $\mathbb{D}_{4h}$ group are labeled in each panel. The instrumental resolution is shown in the upper-right corner of the XY panel. The red lines are fits to a Lorentzian centered at 1.6 meV using the method of maximum likelihood (*37*). The fitted intensity values are $\mathrm{I_{XY}} = 2.7 \pm 0.1$, $\mathrm{I_{X'Y'}} = 2.9 \pm 0.1$, $\mathrm{I_{RR}} = 3.2 \pm 0.1$, $\mathrm{I_{XX}} = 0.91 \pm 0.04$, $\mathrm{I_{X'X'}} = 0.73 \pm 0.04$, and $\mathrm{I_{RL}} = 0.53 \pm 0.04$.

Figure S1 shows the polarization resolved low frequency Raman response function in six scattering geometries within the energy range of 2.5 meV. The data are fitted to a Lorentzian centered at 1.6 meV (convoluted by instrumental resolution). The fitted intensity values are given in figure S1 caption. The intensities can be separated into distinct symmetry channels, $\mathrm{I_{A_{2g}}} = (\mathrm{I_{XY}} + \mathrm{I_{RR}} - \mathrm{I_{X'X'}})/2 = 2.6 \pm 0.1$, $\mathrm{I_{A_{1g}}} = (\mathrm{I_{X'X'}} + \mathrm{I_{RR}} - \mathrm{I_{XY}})/2 = 0.7 \pm 0.1$, $\mathrm{I_{B_{1g}}} = (\mathrm{I_{X'Y'}} + \mathrm{I_{XX}} - \mathrm{I_{RR}})/2 = 0.3 \pm 0.1$, and $\mathrm{I_{B_{2g}}} = (\mathrm{I_{X'X'}} + \mathrm{I_{XY}} - \mathrm{I_{RR}})/2 = 0.1 \pm 0.1$. Hence, the intensity ratios of A_{1g} to A_{2g} channel is $25 \pm 3\%$, B_{1g} to A_{2g} channel is $11 \pm 3\%$, and B_{2g} to A_{2g} channel is $3 \pm 3\%$. Therefore, we claim the observation of the 1.6 meV mode dominantly presenting in the A_{2g} symmetry channel with a weaker intensity leakage into the A_{1g} symmetry channel in the HO phase.

S1.4 Phonon width and leakage at low temperature

The crystal structure of URu_2Si_2 allows 4 Raman active phonon modes, A_{1g}, B_{1g} and $2E_g$ of $\mathbb{D}_{4h}$ group, where the B_{1g} phonon only involves the vibration of Ru atoms (*25, 38*). Figure S2 plots the Raman response function in the X′Y′ scattering geometry at 7 K, containing the B_{1g} phonon centered at 20 meV. The phonon width is composed of its decay rate and inhomogeneous broadening due to stress field (*38, 39*). Hence, the phonon width at low temperature is an indication of crystal quality. It has been demonstrated that stress field on the sample induce local anti-ferromagnetic domains (*11, 40*). Here, the observed phonon width is smaller than the values reported elsewhere for this material (*38, 39*), indicating that the measured surface is stress-free as it is required to study the symmetry of the order parameter in the HO phase.

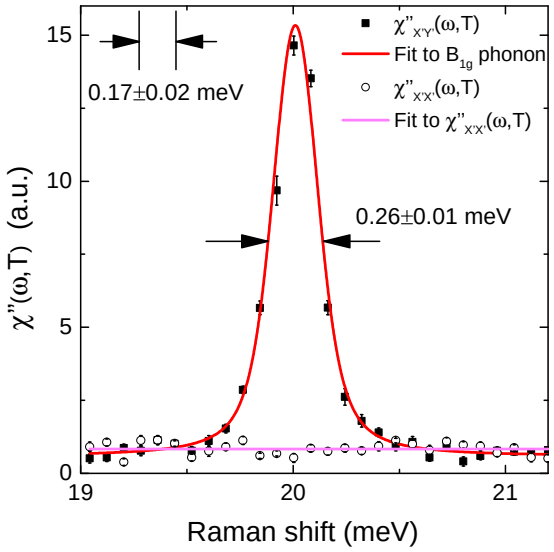

Figure S2: The Raman response function in X′Y′ and X′X′ scattering geometries at 7 K. The data was taken from the same surface as the rest of data presented in this report. The red curve is a fit of the Raman response function in X′Y′ scattering geometry (solid squares) containing the B_{1g} phonon; whereas the pink line is a fit to the Raman response function in X′X′ scattering geometry (open circles) containing no phonon. The observed mode is close to resolution limited, the deconvoluted full-width-at-half-maximum of the B_{1g} phonon is about 0.1 meV. There is no observable B_{1g} phonon leakage into other symmetry channels at 7 K. The instrumental resolution is shown in the upper-left corner.

Recently, a small lattice distortion along the crystallographic a-axis was discovered by X-ray diffraction (*20*), where the observed orthorhombicity is 6.2×10^{-5}. In general, the broken four-fold rotational symmetry allows the B_{1g} phonon at 20.0 meV to leak into other channels. However, within the experimental accuracy, no such orthorhombicity induced phonon leakage was observed in our data. The absence of the phonon leakage is consistent with the tininess of

the orthorhombicity observed by X-ray diffraction (Fig. S2).

S2 The dominant crystal field states of U-5*f* electrons

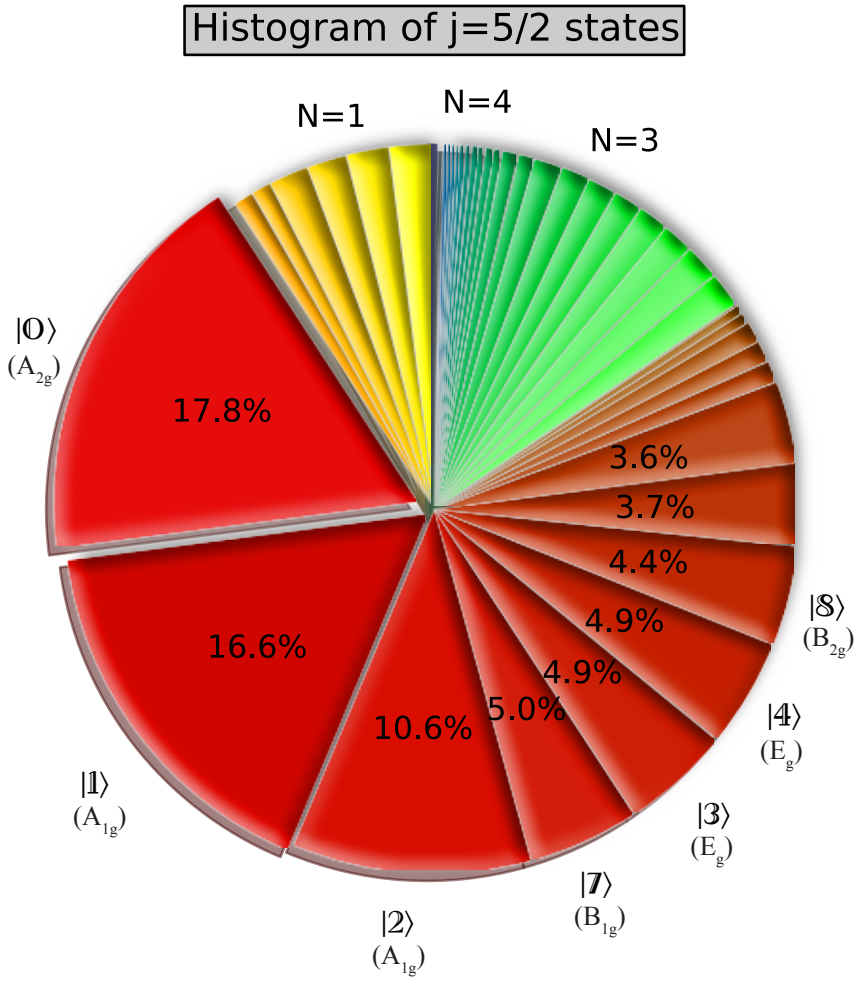

Figure S3: Probabilities to find an U-5f electron in any of the atomic crystal field states, as computed by DFT+DMFT at $T = 20$ K. The states with occupancy 1, 2, 3, and 4 are colored in yellow, red, green, and blue, respectively. The few most important states are labeled in accordance with the table S1.

The U-5*f* electrons have a dual character, i.e., they are partly itinerant and partly localized. In the momentum space, this is reflected in very narrow bands that the U-5*f* states form (mass enhancement of the bands measured in ARPES exceeds density functional theory (DFT) calculated masses by a factor of 10 (*41, 42*)). In the real space picture, their partially itinerant nature

Table S1: The crystal field states of U-5f electrons with two electrons in the $j = 5/2$ subshell, categorized by irreducible representations (IRR) of the $\mathbb{D}_{4h}$ group. These states have total angular moment $J = 4$ and magnetic quantum number M_j runs from $-4 \cdots 4$. The states on the right hand site are labeled by their M_j value, e.g. $|0\rangle \equiv |J = 4, M_j = 0\rangle$

.

IRR	state
A_{2g} (Γ_2)	$\|\mathbb{0}\rangle = \frac{i}{\sqrt{2}}(\|4\rangle - \|-4\rangle)$
A_{1g} ($\Gamma_1^{(1)}$)	$\|\mathbb{1}\rangle = \frac{\cos\theta}{\sqrt{2}}(\|4\rangle + \|-4\rangle) - \sin\theta\,\|0\rangle$
A_{1g} ($\Gamma_1^{(2)}$)	$\|\mathbb{2}\rangle = \frac{\sin\theta}{\sqrt{2}}(\|4\rangle + \|-4\rangle) + \cos\theta\,\|0\rangle$
E_g ($\Gamma_{5,1}^{(1)}$)	$\|\mathbb{3}\rangle = \cos\phi\,\|-3\rangle + \sin\phi\,\|1\rangle$
E_g ($\Gamma_{5,2}^{(1)}$)	$\|\mathbb{4}\rangle = \cos\phi\,\|3\rangle + \sin\phi\,\|-1\rangle$
E_g ($\Gamma_{5,1}^{(2)}$)	$\|\mathbb{5}\rangle = \sin\phi\,\|-3\rangle - \cos\phi\,\|1\rangle$
E_g ($\Gamma_{5,2}^{(2)}$)	$\|\mathbb{6}\rangle = \sin\phi\,\|3\rangle - \cos\phi\,\|-1\rangle$
B_{1g} (Γ_3)	$\|\mathbb{7}\rangle = \frac{1}{\sqrt{2}}(\|2\rangle + \|-2\rangle)$
B_{2g} (Γ_4)	$\|\mathbb{8}\rangle = \frac{i}{\sqrt{2}}(\|2\rangle - \|-2\rangle)$

is reflected in the atomic histogram, which displays finite probability for many atomic states, as opposed to a single state in the atomic limit. In figure S3 we present the real space histogram showing the probability for U-5f electron in the $j = 5/2$ shell to be found in any of the crystal field states. The average number of U-5f electrons within combination of DFT and dynamical mean field theory (DMFT) is $n_f \approx 2.4$, similar to experimental value (*21*), with roughly 0.35 electrons in $j = 7/2$ subshell and roughly 2.05 electrons in $j = 5/2$ subshell. Due to itinerancy, these electrons in $j = 5/2$ shell fluctuate between various atomic configurations, and can be found in any of the 64 possible atomic states. The DFT+DMFT calculation in paramagnetic state, displayed in figure S3, shows that the most probable are configurations with two electrons $N = 2$ (red color), with three $N = 3$ (green color), as well as $N = 1$ (yellow) and $N = 4$ (blue) electrons. Since the $N = 2$ states contribute more than 75% probability, we will here concentrate our discussion here on valence $N = 2$ for $j = 5/2$ electrons. The possible atomic configurations at $N = 2$ are listed in table S1.

S3 The hexadecapole order parameter

For low energy spectroscopies, it is sufficient to introduce a minimal model containing the two lowest energy states in table S1, $|\mathbb{0}\rangle$ and $|\mathbb{1}\rangle$. In this section, we will introduce the hexadecapole order parameter, while in the next section, we will explain the Raman scattering data within the minimal model.

The hexadecapole order parameter results in purely real mixing between $|\mathbb{0}\rangle$ and $|\mathbb{1}\rangle$ in the low energy model, but when extended to other relevant atomic states, which can not be

neglected due to itinerancy of the system, it can have composite nature, i.e. a small admixture of B_{1g} type to leading A_{2g} type order parameter, previously identified in Ref. (*6*). Here, we propose an example of a composite order parameter containing both the A_{2g} and B_{1g} symmetry, and reconcile the Raman scattering results that identify the order parameter of A_{2g} symmetry, and torque experiments (*19*), which require the breaking of four-fold symmetry of the tetragonal lattice in the hidden order state. Such hexadecapolar order parameter can take the form

$$H_{hex} = [(J_x - J_y)(J_x + J_y)(J_xJ_y + J_yJ_x) + (J_xJ_y + J_yJ_x)(J_x + J_y)(J_x - J_y)]\frac{V}{24\sqrt{35}} \quad \text{(S2)}$$

where J_x, J_y are angular momentum operators, V is the hexadecapole order parameter strength, and we assume staggered long range order with wave vector $Q = (0, 0, 1)$. This order parameter is an extension of previously proposed antiferro-hexadecapolar order parameter (*6*), but here extended to a larger Hilbert space outside the low energy model discussed in Ref. (*43*). This order parameter can also be expressed in the form

$$H_{hex} = \frac{V}{24\sqrt{35}}\left[\frac{1}{2i}(J_+^4 - J_-^4) + 2(J_x^2 - J_y^2)\right] \quad \text{(S3)}$$

to emphasize its decomposition into purely A_{2g} type ($J_+^4 - J_-^4$) and B_{1g} type ($J_x^2 - J_y^2$).

It was pointed out in Ref. (*44*) that the A_{2g} part of the local order parameter and the antiferro- staggering lowers the group symmetry from the high temperature $I4/mmm$ (No. 139) to $P4/mnc$ (No. 128). No change in lattice distortion is expected across such a phase transition (*44, 45*), therefore it cannot be detected by X-ray diffraction. The B_{1g} distortion, however, couples to the lattice much stronger than the A_{2g} part, and should be possible to identify. Recently, a small lattice distortion along the crystallographic *a*-axis in the hidden order phase under zero field has been reported by Tonegawa *et al.* (*20*). Such a distortion is in agreement with our proposed hexadecapole order parameter. The tiny lattice distortion arises because the order parameter is staggered in the unit cell, such that the distortion in adjacent layers along c-axis is in opposite direction. Therefore, within a complete unit cell containing two U atoms, the distortion cancels out to first order approximation. Since the B_{1g} part is very weak (i.e., involves higher energy states) and due to this cancellation within a unit cell, only a small distortion can be directly observed by experimental techniques, such as X-ray diffraction.

When this order parameter is written in the space of crystal field levels, the Hamiltonian

takes the form

H_0	$\|\mathbb{0}\rangle$	$\|\mathbb{1}\rangle$	$\|\mathbb{2}\rangle$	$\|\mathbb{7}\rangle$	$\|\mathbb{8}\rangle$	$\|\mathbb{3}\rangle$	$\|\mathbb{4}\rangle$	$\|\mathbb{5}\rangle$	$\|\mathbb{6}\rangle$
$\|\mathbb{0}\rangle$	0	Vh_0	$-Vh_1$	0	Vb_5	0	0	0	0
$\|\mathbb{1}\rangle$	Vh_0	ω_0	0	Vb_4	0	0	0	0	0
$\|\mathbb{2}\rangle$	$-Vh_1$	0	$\varepsilon_{\mathbb{2}}$	Vb_3	0	0	0	0	0
$\|\mathbb{7}\rangle$	0	Vb_4	Vb_3	$\varepsilon_{\mathbb{7}}$	$-Vh_2$	0	0	0	0
$\|\mathbb{8}\rangle$	Vb_5	0	0	$-Vh_2$	$\varepsilon_{\mathbb{8}}$	0	0	0	0
$\|\mathbb{3}\rangle$	0	0	0	0	0	$\varepsilon_{\mathbb{3}}$	Vb_0	$-iVh_3$	$-Vb_2$
$\|\mathbb{4}\rangle$	0	0	0	0	0	Vb_0	$\varepsilon_{\mathbb{3}}$	$-Vb_2$	iVh_3
$\|\mathbb{5}\rangle$	0	0	0	0	0	iVh_3	$-Vb_2$	$\varepsilon_{\mathbb{5}}$	Vb_1
$\|\mathbb{6}\rangle$	0	0	0	0	0	$-Vb_2$	$-iVh_3$	Vb_1	$\varepsilon_{\mathbb{5}}$

(S4)

where h_i are constants that determine the A_{2g} part of the order parameter, and b_i determine its B_{1g} part. Explicitly, h_i and b_i take the form

$$
\begin{aligned}
h_0 &= \sin\theta \\
h_1 &= \cos\theta \\
h_2 &= \frac{3}{2}\sqrt{\frac{5}{7}} \\
h_3 &= \frac{\sqrt{5}}{2} \\
b_0 &= \frac{\sin\phi(3\sqrt{7}\cos\phi + 5\sin\phi)}{6\sqrt{35}} \\
b_1 &= \frac{\cos\phi(5\cos\phi - 3\sqrt{7}\sin\phi)}{6\sqrt{35}} \\
b_2 &= \frac{3\sqrt{7}\cos 2\phi + 5\sin 2\phi}{12\sqrt{35}} \\
b_3 &= \left(\frac{\cos\theta}{2\sqrt{7}} + \frac{\sin\theta}{6\sqrt{5}}\right) \\
b_4 &= \left(\frac{\cos\theta}{6\sqrt{5}} - \frac{\sin\theta}{2\sqrt{7}}\right) \\
b_5 &= \frac{1}{6\sqrt{5}}
\end{aligned}
\tag{S5}
$$

The diagonal elements $\varepsilon_{\mathbb{n}}$ are the energies of the states $|\mathbb{n}\rangle$ relative the ground state $|\mathbb{0}\rangle$, whose energy has been set to zero to simplify the discussion. Note that the low energy sector of states $|\mathbb{0}\rangle$, $|\mathbb{1}\rangle$ and $|\mathbb{2}\rangle$ are coupled only by A_{2g} component of hexadecapole (h_i), while the B_{1g} component adds higher energy states, namely, B_{1g} and B_{2g}.

We will show in the following that while A_{2g} and B_{1g} order parameters alone can not explain the occurrence of the torque in the *ab*-plane (*19, 46*), the presence of both A_{2g} and B_{1g}

fluctuations, and their condensation by a common order parameter Eq. S2, can explain both the angular and temperature dependence of the torque experiment.

S4 The low energy two-states minimal model

In this section, we discuss the Raman scattering phenomena within the minimal model containing the lowest energy A_{2g} and A_{1g} states in table S1, $|\mathbb{0}\rangle$ and $|\mathbb{1}\rangle$, and the order parameter is considered purely real with A_{2g} symmetry.

S4.1 Raman susceptibility in A_{2g} channel and static magnetic susceptibility along *c*-axis

Resonant incoming photon energy, ω_L, is required for coupling to A_{2g} excitations (*23, 26*). The Raman susceptibility in A_{2g} channel can be expressed by

$$\chi_{A_{2g}}(\omega) \propto \int \langle O_{A_{2g}}(\tau) O^{\dagger}_{A_{2g}}(0)\rangle e^{i\omega\tau} d\tau \tag{S6}$$

where $O_{A_{2g}}$ is the Raman operator in the A_{2g} channel, which can be evaluated by

$$O_{A_{2g}} \propto \sum_{jk} c^{\dagger}_j c_k \quad i\sum_l \int d^3\mathbf{r} \int d^3\mathbf{r}' \phi^*_l(\mathbf{r})\phi^*_l(\mathbf{r}') \left(\frac{\partial}{\partial x}\phi_k(\mathbf{r}) \frac{\partial}{\partial y'}\phi^*_j(\mathbf{r}') - \frac{\partial}{\partial y}\phi_k(\mathbf{r}) \frac{\partial}{\partial x'}\phi^*_j(\mathbf{r}') \right) \tag{S7}$$

where $\phi(\mathbf{r})$ are a complete set of one-particle functions.

The magnetic susceptibility along z-axis is

$$\chi^m_z(\omega) \propto \int \langle J_z(\tau) J_z(0)\rangle e^{i\omega\tau} d\tau \tag{S8}$$

Here, J_z can be approximated by the orbital angular momentum operator L_z.

$$L_z \propto \sum_{jk} c^{\dagger}_j c_k \quad i\int d^3\mathbf{r} \phi^*_j(\mathbf{r}) \left(x\frac{\partial}{\partial y} - y\frac{\partial}{\partial x} \right) \phi_k(\mathbf{r}) \tag{S9}$$

Comparing Eq. S7 and S9, we see that $O_{A_{2g}}$ and L_z differ only in the structure of the bare vertex in the brackets, which has the same symmetry properties. Therefore, we have the following relations:

$$\begin{aligned} \langle \mathbb{0}|O_{A_{2g}}|\mathbb{0}\rangle &= \langle \mathbb{0}|J_z|\mathbb{0}\rangle = 0 \\ \langle \mathbb{1}|O_{A_{2g}}|\mathbb{1}\rangle &= \langle \mathbb{1}|J_z|\mathbb{1}\rangle = 0 \\ \langle \mathbb{1}|O_{A_{2g}}|\mathbb{0}\rangle &= \beta \langle \mathbb{1}|J_z|\mathbb{0}\rangle = i\alpha \\ \langle CB|O_{A_{2g}}|\mathbb{0}\rangle &= \beta' \langle CB|J_z|\mathbb{0}\rangle = i\alpha' \end{aligned} \tag{S10}$$

where α, β, α' and β' are real numbers. We see that the matrix elements of $O_{A_{2g}}$ and J_z operators are proportional to each other within the minimal model. This explains the proportionality between $\chi'_{A_{2g}}(0,T)$ and $\chi^m_c(0,T)$ in Fig. 2B of the main text.

S4.2 Effect of the magnetic field along *c*-axis in the HO phase

Consider just the A_{2g} part of the hexadecapole order parameter introduced in Sec. S3, we get the 2×2 low energy sector of Eq. S4:

$$\begin{array}{c|cc} H_0 & |\mathbb{0}\rangle & |\mathbb{1}\rangle \\ \hline |\mathbb{0}\rangle & 0 & V\sin\theta \\ |\mathbb{1}\rangle & V\sin\theta & \omega_0 \end{array} \tag{S11}$$

where $|\mathbb{0}\rangle = \frac{i}{\sqrt{2}}(|4\rangle - |-4\rangle)$ with A_{2g} symmetry, and $|\mathbb{1}\rangle = \frac{\cos\theta}{\sqrt{2}}(|4\rangle + |-4\rangle) - \sin\theta\,|0\rangle$ with A_{1g} symmetry, are the singlet crystal field states of the U-5f electrons. Notice that we have absorbed the $\sin\theta$ factor into V in the main text.

From perturbation theory, the perturbed states up to second order in V are:

$$\begin{aligned} |\aleph\rangle &= (1 - \frac{V^2\sin^2\theta}{2\omega_0^2})\,|\mathbb{0}\rangle + \frac{V\sin\theta}{\omega_0}\,|\mathbb{1}\rangle + \mathcal{O}(V^3) \\ |\beth\rangle &= \frac{-V\sin\theta}{\omega_0}\,|\mathbb{0}\rangle + (1 - \frac{V^2\sin^2\theta}{2\omega_0^2})\,|\mathbb{1}\rangle + \mathcal{O}(V^3) \end{aligned} \tag{S12}$$

Notice that V can take up positive or negative values. In the following, we will use the notation:

$$\begin{aligned} |\aleph^+\rangle &= (1 - \frac{V^2\sin^2\theta}{2\omega_0^2})\,|\mathbb{0}\rangle + \frac{|V|\sin\theta}{\omega_0}\,|\mathbb{1}\rangle + \mathcal{O}(V^3) \\ |\aleph^-\rangle &= (1 - \frac{V^2\sin^2\theta}{2\omega_0^2})\,|\mathbb{0}\rangle - \frac{|V|\sin\theta}{\omega_0}\,|\mathbb{1}\rangle + \mathcal{O}(V^3) \end{aligned} \tag{S13}$$

to distinguish the right- and left-handed states.

Following similar construction, but consider now the Hamiltonian in the presence of B-field in z-direction (along c-axis), that is $H = H_0 + V\sin\theta + g\mu_B J_z B$, where g is Landé g-factor, μ_B is Bohr magneton, J_z is the azimuthal angular momentum, and B is the field strength along z. We can now write the Hamiltonian in the representation of crystal field states in our minimal model:

$$\begin{array}{c|cc} H & |\mathbb{0}\rangle & |\mathbb{1}\rangle \\ \hline |\mathbb{0}\rangle & 0 & V\sin\theta - i\gamma B \\ |\mathbb{1}\rangle & V\sin\theta + i\gamma B & \omega_0 \end{array} \tag{S14}$$

and hence the excitation energy in the presence of the field is

$$E_{A_{2g}}(B,V) = \sqrt{\omega_0^2 + 4V^2\sin^2\theta + (2\gamma B)^2} \tag{S15}$$

Inserting states $|\mathbb{0}\rangle$ and $|\mathbb{1}\rangle$ in table S1 leads to $\gamma = 4\cos\theta g\mu_B$. The field dependence of the same excitation observed by neutron scattering experiment is consistent with Eq. S15 with $2\gamma \approx 0.114$ meV/T, leading to $\cos\theta \approx 0.25$ (*29*). Given that URu_2Si_2 is in a mixed-valent state, the numbers from such localized calculations should be regarded as semi-quantitative. However, the symmetry considerations are general.

S4.3 The Raman intensity of the A_{2g} in-gap mode

From Eq. S12, we find that the transition amplitude between states $|\aleph\rangle$ and $|\beth\rangle$ in the A_{2g} channel is:

$$\begin{aligned}\langle\beth|O_{A_{2g}}|\aleph\rangle &= \left(1-\frac{V^2\sin^2\theta}{\omega_0^2}\right)\langle\mathbb{1}|O_{A_{2g}}|\mathbb{0}\rangle - \frac{V^2\sin^2\theta}{\omega_0^2}\langle\mathbb{0}|O_{A_{2g}}|\mathbb{1}\rangle + \mathcal{O}(V^4)\\ &= \langle\mathbb{1}|O_{A_{2g}}|\mathbb{0}\rangle - \frac{V^2\sin^2\theta}{\omega_0^2}\Big(\langle\mathbb{1}|O_{A_{2g}}|\mathbb{0}\rangle + \langle\mathbb{0}|O_{A_{2g}}|\mathbb{1}\rangle\Big) + \mathcal{O}(V^4)\\ &= \langle\mathbb{1}|O_{A_{2g}}|\mathbb{0}\rangle + \mathcal{O}(V^4)\end{aligned} \tag{S16}$$

Therefore, the intensity in the A_{2g} channel to the lowest order in V is

$$I_{A_{2g}} = |\,\langle\beth|O_{A_{2g}}|\aleph\rangle\,|^2 = |\,\langle\mathbb{1}|O_{A_{2g}}|\mathbb{0}\rangle\,|^2 + \mathcal{O}(V^4) \tag{S17}$$

Here we have used $\langle\mathbb{0}|O_{A_{2g}}|\mathbb{0}\rangle = \langle\mathbb{1}|O_{A_{2g}}|\mathbb{1}\rangle = 0$ by symmetry selection rules, and $\langle\mathbb{1}|O_{A_{2g}}|\mathbb{0}\rangle = (\langle\mathbb{0}|O_{A_{2g}}|\mathbb{1}\rangle)^* = i\alpha$ from Eq. S10.

S4.4 The "leakage" intensity of the in-gap mode into the A_{1g} channel

From symmetry arguments, $\langle\mathbb{1}|O_{A_{1g}}|\mathbb{0}\rangle = \langle\mathbb{0}|O_{A_{1g}}|\mathbb{1}\rangle = 0$, where $O_{A_{1g}}$ is the Raman operator for the A_{1g} channel. From Eq. S12 we find that the transition amplitude between states $|\aleph\rangle$ and $|\beth\rangle$ in the A_{1g} channel is:

$$\begin{aligned}\langle\beth|O_{A_{1g}}|\aleph\rangle &= \frac{V\sin\theta}{\omega_0}\langle\mathbb{0}|O_{A_{1g}}|\mathbb{0}\rangle - \frac{V\sin\theta}{\omega_0}\langle\mathbb{1}|O_{A_{1g}}|\mathbb{1}\rangle + \mathcal{O}(V^3)\\ &= \frac{V\sin\theta}{\omega_0}\Big(\langle\mathbb{0}|O_{A_{1g}}|\mathbb{0}\rangle - \langle\mathbb{1}|O_{A_{1g}}|\mathbb{1}\rangle\Big) + \mathcal{O}(V^3)\end{aligned} \tag{S18}$$

Therefore, the intensity in the A_{1g} channel is

$$I_{A_{1g}} = |\,\langle\beth|O_{A_{1g}}|\aleph\rangle\,|^2 \sim \frac{V^2\sin^2\theta}{\omega_0^2}\Big(\langle\mathbb{0}|O_{A_{1g}}|\mathbb{0}\rangle - \langle\mathbb{1}|O_{A_{1g}}|\mathbb{1}\rangle\Big)^2 \tag{S19}$$

We see that the intensity of the "leakage" into A_{1g} channel is proportional to the square of the order parameter, $V^2\sin^2\theta$. Here, the temperature dependence of the gap function shows that the order parameter almost fully develops below $\sim \frac{1}{2}T_{\text{HO}}$ (Fig. 2C).

Moreover, in the resonant regime, required for coupling to the A_{2g} excitations, the Raman operators scatter photons via intermediate states (Fig. S4). Hence, the intensity of the "leakage" mode critically depend on the laser excitation energy, ω_L, because of possible cancellation of the term $\Big(\langle\mathbb{0}|O_{A_{1g}}|\mathbb{0}\rangle - \langle\mathbb{1}|O_{A_{1g}}|\mathbb{1}\rangle\Big)^2$. Similarly, the ratio of $I_{A_{1g}}/I_{A_{2g}}$ will depend ω_L.

S4.5 Beyond the minimal model

It is pointed out in Sec. S2 that another state with A_{1g} symmetry

$$|\beth\rangle = \frac{\sin\theta}{\sqrt{2}}(|4\rangle + |-4\rangle) + \cos\theta\,|0\rangle \tag{S20}$$

is comparable to $|\daleth\rangle$ in terms of energy. The Hamiltonian including this states and the A_{2g} part of the order parameter is:

H_0	$\|\gimel\rangle$	$\|\daleth\rangle$	$\|\beth\rangle$
$\|\gimel\rangle$	0	$V\sin\theta$	$-V\cos\theta$
$\|\daleth\rangle$	$V\sin\theta$	ω_0	0
$\|\beth\rangle$	$-V\cos\theta$	0	$\varepsilon_{\beth}$

(S21)

where $\varepsilon_{\beth}$ is the energy of state $|\beth\rangle$. The perturbed HO eigenfunctions up to second order in V are:

$$\begin{aligned}
|\aleph\rangle &= \left(1 - \frac{V^2\sin^2\theta}{2\omega_0^2} - \frac{V^2\cos^2\theta}{2\varepsilon_{\beth}^2}\right)|\gimel\rangle - \frac{V\sin\theta}{\omega_0}|\daleth\rangle + \frac{V\cos\theta}{\varepsilon_{\beth}}|\beth\rangle + \mathcal{O}(V^3)\\
|\beth\rangle &= \frac{V\sin\theta}{\omega_0}|\gimel\rangle + \left(1 - \frac{V^2\sin^2\theta}{2\omega_0^2}\right)|\daleth\rangle + V^2\left(\frac{\sin\theta\cos\theta}{\omega_0(\varepsilon_{\beth}-\omega_0)}\right)|\beth\rangle + \mathcal{O}(V^3)\\
|\gimel\rangle &= \frac{-V\cos\theta}{\varepsilon_{\beth}}|\gimel\rangle - V^2\left(\frac{\sin\theta\cos\theta}{\varepsilon_{\beth}(\varepsilon_{\beth}-\omega_0)}\right)|\daleth\rangle + \left(1 - \frac{V^2\cos^2\theta}{2\varepsilon_{\beth}^2}\right)|\beth\rangle + \mathcal{O}(V^3)
\end{aligned} \tag{S22}$$

Since both states $|\daleth\rangle$ and $|\beth\rangle$ are of A_{1g} symmetry, one would expect two resonances in the A_{2g} channel. However, we show in the following that only one resonance resulting from transition $|\aleph\rangle \to |\gimel\rangle$ is expected.

From Eq. S22, the resonances in the A_{2g} channel are:

$$\begin{aligned}
\langle\gimel|O_{A_{2g}}|\aleph\rangle &= \left(1 - \frac{V^2\sin^2\theta}{\omega_0^2} - \frac{V^2\cos^2\theta}{2\varepsilon_{\beth}^2}\right)\langle\daleth|O_{A_{2g}}|\gimel\rangle - \frac{V^2\sin^2\theta}{\omega_0^2}\langle\gimel|O_{A_{2g}}|\daleth\rangle\\
&\quad + V^2\left(\frac{\sin\theta\cos\theta}{\omega_0(\varepsilon_{\beth}-\omega_0)}\right)\langle\beth|O_{A_{2g}}|\gimel\rangle + V^2\frac{\sin\theta\cos\theta}{\omega_0\varepsilon_{\beth}}\langle\gimel|O_{A_{2g}}|\beth\rangle + \mathcal{O}(V^4)\\
&= \langle\daleth|O_{A_{2g}}|\gimel\rangle + \mathcal{O}(V^2)
\end{aligned} \tag{S23}$$

$$\begin{aligned}
\langle\gimel|O_{A_{2g}}|\aleph\rangle &= \left(1 - \frac{V^2\sin^2\theta}{2\omega_0^2} - \frac{V^2\cos^2\theta}{\varepsilon_{\beth}^2}\right)\langle\beth|O_{A_{2g}}|\gimel\rangle - \frac{V^2\cos^2\theta}{\varepsilon_{\beth}^2}\langle\gimel|O_{A_{2g}}|\beth\rangle\\
&\quad - V^2\left(\frac{\sin\theta\cos\theta}{\varepsilon_{\beth}(\varepsilon_{\beth}-\omega_0)}\right)\langle\daleth|O_{A_{2g}}|\gimel\rangle + V^2\frac{\sin\theta\cos\theta}{\omega_0\varepsilon_{\beth}}\langle\gimel|O_{A_{2g}}|\daleth\rangle + \mathcal{O}(V^4)\\
&= \langle\beth|O_{A_{2g}}|\gimel\rangle + \mathcal{O}(V^2)
\end{aligned} \tag{S24}$$

However, the second resonance, $\langle\gimel|O_{A_{2g}}|\aleph\rangle$, is not allowed due to angular momentum conservation. A two photon process such as Raman scattering can only promote states with $\Delta J_z =$

$0, \pm 2\hbar$, where J_z is the angular momentum of the states involved in the transition. In the limit of $\theta \to 0$, only transition $|\mathbb{0}\rangle \to |\mathbb{1}\rangle$ is allowed in the RR scattering geometry, where there is no angular momentum transfer between the incident and scattered photon (Fig. S4). On the other hand, the transition $|\mathbb{0}\rangle \to |\mathbb{2}\rangle$ requires $\Delta J_z = \pm 4\hbar$ and only enters in Raman scattering as high order process. Therefore, we conclude that the resonance in Raman scattering A_{2g} channel is resulted mainly from transition $|\mathbb{0}\rangle \to |\mathbb{1}\rangle$, and it is sufficient to introduce these two lowest lying states to explain the Raman scattering data.

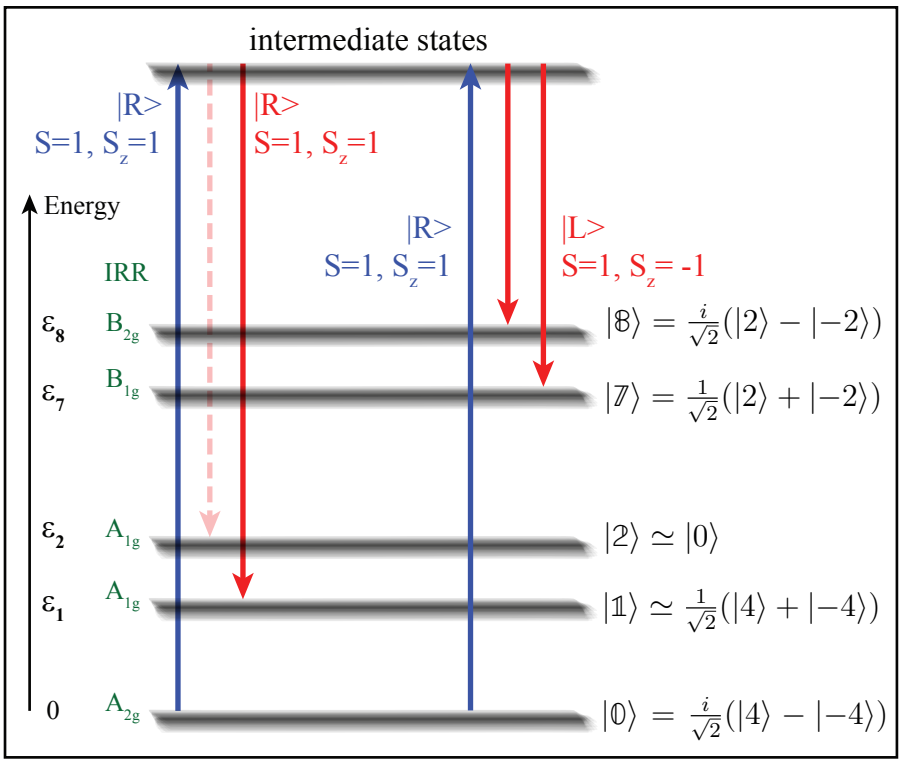

Figure S4: Schematic drawing of the Raman selection rules due to angular momentum conservation. The left hand side shows the energy and irreducible representations of $\mathbb{D}_{4h}$ group of the crystal field states, and the right hand side shows these states in the two electron wave function representation. Notice that $|\mathbb{1}\rangle$ and $|\mathbb{2}\rangle$ have been approximated by assuming small θ. The blue (red) arrow denotes the direction of electronic transition due to incident (scattered) circularly polarized light, where the dashed red line is forbidden due to violation of angular momentum conservation.

The hexadecapole coupling operator is proportional to J^4, therefore in the limit of $\theta \to 0$, it will couple only the $|\mathbb{0}\rangle$ and $|\mathbb{2}\rangle$ states, and Raman scattering would not be able to see the leakage in the A_{1g} channel. However for small but non-zero θ, the transition amplitudes in the

A_{1g} channel consist of two transitions:

$$\begin{aligned}\langle \beth | O_{A_{1g}} | \aleph \rangle &= \frac{V \sin\theta}{\omega_0} \langle \mathbb{0} | O_{A_{1g}} | \mathbb{0} \rangle - \frac{V \sin\theta}{\omega_0} \langle \mathbb{1} | O_{A_{1g}} | \mathbb{1} \rangle + \mathcal{O}(V^3) \\ &= \frac{V \sin\theta}{\omega_0} \Big(\langle \mathbb{0} | O_{A_{1g}} | \mathbb{0} \rangle - \langle \mathbb{1} | O_{A_{1g}} | \mathbb{1} \rangle \Big) + \mathcal{O}(V^3)\end{aligned} \tag{S25}$$

$$\begin{aligned}\langle \gimel | O_{A_{1g}} | \aleph \rangle &= \frac{-V \cos\theta}{\varepsilon_{\beth}} \langle \mathbb{0} | O_{A_{1g}} | \mathbb{0} \rangle + \frac{V \cos\theta}{\varepsilon_{\beth}} \langle \beth | O_{A_{1g}} | \beth \rangle + \mathcal{O}(V^3) \\ &= \frac{-V \cos\theta}{\varepsilon_{\beth}} \Big(\langle \mathbb{0} | O_{A_{1g}} | \mathbb{0} \rangle - \langle \beth | O_{A_{1g}} | \beth \rangle \Big) + \mathcal{O}(V^3)\end{aligned} \tag{S26}$$

The two transitions have the same order of V, but different energy. The fact that we don't see the transition $|\aleph\rangle \to |\gimel\rangle$ is possibly because its energy is higher than the gap and therefore, it is an over-damped excitation.

S4.6 Leakage intensity due to broken C_4 symmetry

Recently, there have been reports on broken four-fold rotational symmetry observed by magnetic torque (*19*) and X-ray diffraction (*20*). Such symmetry breaking lowers the group symmetry from $\mathbb{C}_{4h}$ to $\mathbb{C}_{2h}$. In the $\mathbb{C}_{2h}$ group, RL is no longer a "proper" scattering geometry. Therefore, it is expected to see a leakage intensity of the 1.6 meV mode into the RL geometry.

S5 Magnetic torque in the ordered state with field in *xy*-plane

In the following, we explain that the four-fold rotational symmetry breaking observed in magnetic torque experiment can be full accounted for by the composite hexadecapole order parameter (Eq. S2).

Using perturbation theory, the ground state local wave function in the hexadecapole ordered state is

$$|\aleph\rangle = |\mathbb{0}\rangle\, a_0 - |\mathbb{1}\rangle\, a_1 + |\beth\rangle\, a_2 + |\daleth\rangle\, a_7 - |\gimel\rangle\, a_8 \tag{S27}$$

where coefficients up to the second order in V are given by

$$\begin{aligned} a_0 &= \left(1 - \frac{1}{2}\frac{V^2 h_0^2}{\omega_0^2} - \frac{1}{2}\frac{V^2 h_1^2}{\varepsilon_{2}^2} - \frac{1}{2}\frac{V^2 b_5^2}{\varepsilon_{8}^2}\right) \\ a_1 &= \frac{V h_0}{\omega_0} \\ a_2 &= \frac{V h_1}{\varepsilon_{2}} \\ a_7 &= V^2 \left(\frac{h_0 b_4}{\omega_0 \varepsilon_{7}} - \frac{h_1 b_3}{\varepsilon_{7}\varepsilon_{2}} - \frac{h_2 b_5}{\varepsilon_{7}\varepsilon_{8}}\right) \\ a_8 &= \frac{V b_5}{\varepsilon_{8}} \end{aligned} \tag{S28}$$

Notice that at small V, $a_7 \ll a_8 \ll a2 \ll a1$. The minimal model introduced in Ref. (*43*) contained only a_0 and a_1, and their coupling is only through the A_{2g} part of the order parameter (constants h_i). The B_{1g} part of the order parameter mixes in B_{2g} state at the first order (although small because $\omega_0/\varepsilon_{8} \ll 1$) and B_{1g} at the second order in V (which is also small because $\omega_0/\varepsilon_{7} \ll 1$).

If the magnetic field **B** is in *xy*-plane (but not exactly along the x or y axis), the magnetization **M** points in different direction than **B**, hence there is finite torque along z axis, $\vec{\tau} = \mathbf{M} \times \mathbf{B}$. To compute the torque, we first evaluate the change of the hexadecapole wave function $|\aleph\rangle$ due to magnetic field perturbation in the *xy*-plane $\delta H_B = -J_x \cos\vartheta - J_y \sin\vartheta$ (notice that the ϑ here is the magnetic field angle, different from the crystal field angle θ defined in Eq. S4). The change takes the form

$$|\delta\aleph\rangle \approx -\frac{B}{\varepsilon_{0} - \varepsilon_{3}}\left[p^*(\vartheta)\,|3\rangle + p(\vartheta)\,|4\rangle\right] - \frac{B}{\varepsilon_{0} - \varepsilon_{5}}\left[\widetilde{p}^*(\vartheta)\,|5\rangle + \widetilde{p}(\vartheta)\,|6\rangle\right] \tag{S29}$$

where

$$\begin{aligned} p(\vartheta) &\equiv c\cos\phi e^{i\vartheta} + d^* e^{-i\vartheta} \\ \widetilde{p}(\vartheta) &\equiv \widetilde{c}\sin\phi e^{i\vartheta} + d^* e^{-i\vartheta} \end{aligned} \tag{S30}$$

with

$$\begin{aligned} c &\equiv i a_0 - \alpha a_1 + \widetilde{\alpha} a_2 \\ d &\equiv a_7\beta + i a_8 \beta' \\ \widetilde{c} &\equiv i a_0 - \alpha' a_1 + \widetilde{\alpha}' a_2 \\ \widetilde{d} &\equiv a_7\widetilde{\beta}' + i a_8 \widetilde{\beta} \end{aligned} \tag{S31}$$

We used the short-notation for constants determined by the crystal field angle θ and ϕ:

$$\begin{aligned}
\alpha &= \cos\theta - \sqrt{5}\sin\theta\tan\phi \\
\alpha' &= \cos\theta + \sqrt{5}\sin\theta\cot\phi \\
\widetilde{\alpha} &= \sin\theta + \sqrt{5}\cos\theta\tan\phi \\
\widetilde{\alpha}' &= \sin\theta - \sqrt{5}\cos\theta\cot\phi \\
\beta &= (\sqrt{7}\cos\phi + 3\sin\phi)/2 \\
\beta' &= (\sqrt{7}\cos\phi - 3\sin\phi)/2 \\
\widetilde{\beta} &= (\sqrt{7}\sin\phi + 3\cos\phi)/2 \\
\widetilde{\beta}' &= (\sqrt{7}\sin\phi - 3\cos\phi)/2
\end{aligned} \tag{S32}$$

and the constants determined by the crystal field level angle θ: Here we neglected the change of the energies of the E_g states due to the hexadecapolar order, which can be neglected at this order. While the energy of the A_{2g} state $|\mathbb{0}\rangle$ is lifted to $\varepsilon_{\mathbb{0}}$.

The magnetization is proportional to

$$\begin{aligned}
M_\alpha = \langle J_\alpha \rangle &= \left(\langle \aleph| + \langle \delta\aleph|\right) J_\alpha \left(|\aleph\rangle + |\delta\aleph\rangle\right) \\
&= \langle \aleph| J_\alpha |\aleph\rangle + 2\mathrm{Re}(\langle \aleph| J_\alpha |\delta\aleph\rangle) + \langle \delta\aleph| J_\alpha |\delta\aleph\rangle
\end{aligned} \tag{S33}$$

The first term vanishes. The linear in B contribution will come from the second term $\langle \aleph| J_\alpha |\delta\aleph\rangle$, which will be computed below.

We notice that $J_z|\mathbb{0}\rangle$ gives $|\mathbb{1}\rangle$ states, while $J_x|\mathbb{0}\rangle$ gives $|E_g\rangle$ states, hence when magnetic field points in z-direction, there is no magnetic moment in x-direction, and vice-versa. This statement remains valid even in the ordered state. As a consequence, the torque in the first order perturbation theory (B^2 term) can only be proportional to $\sin 2\vartheta$, when B field is swiped in the *xz*-plane.

We also need J_x and J_y acting on the ground state, i.e.,

$$\begin{aligned}
J_x|\aleph\rangle &= p^*(0)|\beth\rangle + p(0)|\gimel\rangle + \widetilde{p}^*(0)|\daleth\rangle + \widetilde{p}(0)|\mathbb{6}\rangle \\
J_y|\aleph\rangle &= p^*(\pi/2)|\beth\rangle + p(\pi/2)|\gimel\rangle + \widetilde{p}^*(\pi/2)|\daleth\rangle\, \widetilde{p}(\pi/2)|\mathbb{6}\rangle
\end{aligned} \tag{S34}$$

We now compute $M_x/2 = \langle \aleph| J_x |\delta\aleph\rangle$ and $M_y/2 = \langle \aleph| J_y |\delta\aleph\rangle$, which are given by

$$\begin{aligned}
M_x = &\frac{4B\cos\vartheta}{\varepsilon_{\beth} - \varepsilon_{\mathbb{0}}}\left(|c|^2\cos^2\phi + |d|^2 + 2\cos\phi\,\mathrm{Re}(cd) +\right) - \frac{8B\sin\vartheta}{\varepsilon_{\beth} - \varepsilon_{\mathbb{0}}}\cos\phi\,\mathrm{Im}(cd) \\
&+\frac{4B\cos\vartheta}{\varepsilon_{\daleth} - \varepsilon_{\mathbb{0}}}\left(|\widetilde{c}|^2\sin^2\phi + |\widetilde{d}|^2 + 2\sin\phi\,\mathrm{Re}(\widetilde{c}\widetilde{d})\right) - \frac{8B\sin\vartheta}{\varepsilon_{\daleth} - \varepsilon_{\mathbb{0}}}\sin\phi\,\mathrm{Im}(\widetilde{c}\widetilde{d})
\end{aligned} \tag{S35}$$

$$\begin{aligned}
M_y = &\frac{4B\sin\vartheta}{\varepsilon_{\beth} - \varepsilon_{\mathbb{0}}}\left(|c|^2\cos^2\phi + |d|^2 - 2\cos\phi\,\mathrm{Re}(cd)\right) - \frac{8B\cos\vartheta}{\varepsilon_{\beth} - \varepsilon_{\mathbb{0}}}\cos\phi\,\mathrm{Im}(cd) \\
&+\frac{4B\sin\vartheta}{\varepsilon_{\daleth} - \varepsilon_{\mathbb{0}}}\left(+|\widetilde{c}|^2\sin^2\phi + |\widetilde{d}|^2 - 2\sin\phi\,\mathrm{Re}(\widetilde{c}\widetilde{d})\right) - \frac{8B\cos\vartheta}{\varepsilon_{\daleth} - \varepsilon_{\mathbb{0}}}\sin\phi\,\mathrm{Im}(\widetilde{c}\widetilde{d})
\end{aligned} \tag{S36}$$

The torque $\tau_z = B(M_x \sin\vartheta - M_y \cos\vartheta)$ on a given site is therefore

$$\tau_z = 8B^2 \sin 2\vartheta \left(\frac{\cos\phi\, \mathrm{Re}(cd)}{\varepsilon_{\mathbb{3}} - \varepsilon_{\mathbb{0}}} + \frac{\sin\phi\, \mathrm{Re}(\widetilde{c}\widetilde{d})}{\varepsilon_{\mathbb{5}} - \varepsilon_{\mathbb{0}}} \right) + 8B^2 \cos 2\vartheta \left(\frac{\cos\phi\, \mathrm{Im}(cd)}{\varepsilon_{\mathbb{3}} - \varepsilon_{\mathbb{0}}} + \frac{\sin\phi\, \mathrm{Im}(\widetilde{c}\widetilde{d})}{\varepsilon_{\mathbb{5}} - \varepsilon_{\mathbb{0}}} \right) \tag{S37}$$

Next we work out the coefficients

$$\begin{aligned}
\mathrm{Re}(cd) &= -\frac{V b_5}{\varepsilon_{\mathbb{8}}}\, \beta' \\
\mathrm{Im}(cd) &= V^2 \left(-\frac{h_0 b_5}{\omega_0 \varepsilon_{\mathbb{8}}} \alpha\beta' + \frac{h_1 b_5}{\varepsilon_{\mathbb{2}} \varepsilon_{\mathbb{8}}} \widetilde{\alpha}\beta' + \frac{h_0 b_4}{\omega_0\, \varepsilon_{\mathbb{7}}} \beta - \frac{h_1 b_3}{\varepsilon_{\mathbb{7}} \varepsilon_{\mathbb{2}}} \beta - \frac{h_2 b_5}{\varepsilon_{\mathbb{7}} \varepsilon_{\mathbb{8}}} \beta \right) \\
\mathrm{Re}(\widetilde{c}\widetilde{d}) &= -\frac{V b_5}{\varepsilon_{\mathbb{8}}}\, \widetilde{\beta} \\
\mathrm{Im}(\widetilde{c}\widetilde{d}) &= V^2 \left(-\frac{h_0 b_5}{\omega_0 \varepsilon_{\mathbb{8}}} \alpha'\widetilde{\beta} + \frac{h_1 b_5}{\varepsilon_{\mathbb{2}} \varepsilon_{\mathbb{8}}} \widetilde{\alpha}'\widetilde{\beta} + \frac{h_0 b_4}{\omega_0\, \varepsilon_{\mathbb{7}}} \widetilde{\beta}' - \frac{h_1 b_3}{\varepsilon_{\mathbb{7}} \varepsilon_{\mathbb{2}}} \widetilde{\beta}' - \frac{h_2 b_5}{\varepsilon_{\mathbb{7}} \varepsilon_{\mathbb{8}}} \widetilde{\beta}' \right)
\end{aligned} \tag{S38}$$

We notice that $\mathrm{Re}(cd)$ is odd function of V. In the ordered phase, the two U atoms in the unit cell have opposite value of V and hence this term vanishes. The second term $\mathrm{Im}(cd)$ is even function of V and remains non-zero in the staggered hexadecapolar phase. We hence obtain the torque of the form

$$\tau_z = \frac{8B^2V^2}{\varepsilon_{eg} - \varepsilon_{\mathbb{0}}} \cos 2\vartheta \left(\frac{h_0 b_4}{\omega_0\, \varepsilon_{\mathbb{7}}} \gamma_3 - \frac{h_0 b_5}{\omega_0 \varepsilon_{\mathbb{8}}} \gamma_1 + \frac{h_1 b_5}{\varepsilon_{\mathbb{2}} \varepsilon_{\mathbb{8}}} \gamma_2 - \frac{h_1 b_3}{\varepsilon_{\mathbb{7}} \varepsilon_{\mathbb{2}}} \gamma_3 - \frac{h_2 b_5}{\varepsilon_{\mathbb{7}} \varepsilon_{\mathbb{8}}} \gamma_3 \right) \tag{S39}$$

where γ's are some real numbers of order unity

$$\begin{aligned}
\gamma_1 &= \left(\alpha\beta'\, \cos\phi \frac{\varepsilon_{eg} - \varepsilon_{\mathbb{0}}}{\varepsilon_{\mathbb{3}} - \varepsilon_{\mathbb{0}}} + \alpha'\widetilde{\beta}\, \sin\phi \frac{\varepsilon_{eg} - \varepsilon_{\mathbb{0}}}{\varepsilon_{\mathbb{5}} - \varepsilon_{\mathbb{0}}} \right) \\
\gamma_2 &= \left(\widetilde{\alpha}\beta' \cos\phi \frac{\varepsilon_{eg} - \varepsilon_{\mathbb{0}}}{\varepsilon_{\mathbb{3}} - \varepsilon_{\mathbb{0}}} + \widetilde{\alpha}'\widetilde{\beta} \sin\phi \frac{\varepsilon_{eg} - \varepsilon_{\mathbb{0}}}{\varepsilon_{\mathbb{5}} - \varepsilon_{\mathbb{0}}} \right) \\
\gamma_3 &= \left(\beta \cos\phi \frac{\varepsilon_{eg} - \varepsilon_{\mathbb{0}}}{\varepsilon_{\mathbb{3}} - \varepsilon_{\mathbb{0}}} + \widetilde{\beta}' \sin\phi \frac{\varepsilon_{eg} - \varepsilon_{\mathbb{0}}}{\varepsilon_{\mathbb{5}} - \varepsilon_{\mathbb{0}}} \right)
\end{aligned} \tag{S40}$$

and we choose $\varepsilon_{eg} = (\varepsilon_{\mathbb{3}} + \varepsilon_{\mathbb{5}})/2$.

This is the central result of this section and shows that the hexadecapolar order parameter Eq. S2 can explain the $\cos(2\vartheta)$ oscillation observed in the magnetic torque experiment (*19*). It also explains the observed linear temperature dependence, because V is the order parameter and has a $(1 - T/T_c)^{1/2}$ dependence.

Notice that finite value of torque is a result of the interference term between A_{2g} and B_{1g} part of the order parameter ($h_i b_j$ terms). If B_{1g} part vanishes, there is no torque. If B_{1g} is finite but A_{2g} vanishes, $\mathrm{Re}(cd)$ is nonzero, but since it is proportional to V, it vanishes when staggered

phase is considered. It is therefore crucial to consider such composite order parameter, which contains primary A_{2g} part, and subleading B_{1g} part.

The perturbation theory to higher order gives torque per site to be

$$\tau_z \propto c_1 B^4 (1 - c_0 V^2) \sin 4\vartheta + c_2 B^4 V \cos 4\vartheta. \tag{S41}$$

The second term is odd in V, and hence cancels in the staggered phase, and we are left with the 4ϑ-oscillations of torque of the form

$$\tau_z \propto B^4 (1 - c_0 V^2) \sin 4\vartheta \tag{S42}$$

as seen in the magnetic torque experiment in the ordered state (*19*).